Modeling Images and Spectra of a Solar Flare Observed by RHESSI on 20 February 2002

Linhui Sui (lhsui@stars.gsfc.nasa.gov)
CUA & Laboratory for Astronomy and Solar Physics, NASA Goddard Space Flight Center, Greenbelt, MD 20771, U.S.A.

Gordon D. Holman (holman@stars.gsfc.nasa.gov)
and Brian R. Dennis (brian.r.dennis.1@gsfc.nasa.gov)
Laboratory for Astronomy and Solar Physics, NASA Goddard Space Flight Center, Greenbelt, MD 20771, U.S.A.

Säm Krucker (krucker@ssl.berkeley.edu)
Space Science Lab, University of California at Berkeley, Berkeley, CA 94720, U.S.A.

Richard A. Schwartz (richard.schwartz@gsfc.nasa.gov)
and Kim Tolbert (kim.tolbert@gsfc.nasa.gov)
SSAI & Laboratory for Astronomy and Solar Physics, NASA Goddard Space Flight Center, Greenbelt, MD 20771, U.S.A.

Abstract. We have analyzed a C7.5 limb flare observed by RHESSI on 20 February 2002. The RHESSI images appear to show two footpoints and a looptop source. Our goal was to determine if the data are consistent with a simple steady-state model in which high-energy electrons are continuously injected at the top of a semicircular flare loop. A comparison of the RHESSI images with simulated images from the model has made it possible for us to identify spurious sources and fluxes in the RHESSI images. We find the RHESSI results are in many aspects consistent with the model if a thermal source is included between the loop footpoints, but there is a problem with the spectral index of the looptop source. The thermal source between the footpoints is likely to be a low-lying loop interacting with the northern footpoint of a higher loop containing the looptop source.

Keywords: Flare: X-ray: Bremsstrahlung

1. Introduction

The study of hard X-ray emission is important for understanding electron acceleration and transportation in flares. Most observations of solar hard X-rays have been obtained with poor spectral and spatial resolution. Years of *Yohkoh* HXT observations indicate that many types of hard X-ray sources exist, even in a single flare (Masuda, 2002). For this reason, imaging spectroscopy is very important for investigating individual sources in flares, demanding X-ray data with high spatial, spectral and temporal resolution. The Ramaty High Energy

Solar Spectroscopic Imager (RHESSI), launched on 5 February 2002, is now obtaining high spatial (∼2″), spectral (∼1 keV) and temporal (tens of milliseconds) resolution data in 3 keV – 17 MeV X-rays and γ-rays. All these new features o er a dramatic improvement in studying the hard X-ray emission from flares.

In order to interpret RHESSI images and spectra, we established flare models (Holman *et al.*, 2001; 2002) based on *Yohkoh* HXT observations of looptop sources (Masuda, 1994). We apply one of these models to a flare observed by RHESSI on 20 February 2002. We first compute model images with flare parameters derived from the observational data. We then obtain simulated RHESSI images and spectra using the computed model images as input. Finally, we compare the simulated images and spectra with RHESSI results. This method not only tests our model, but enables us to test the RHESSI imaging software as well.

2. Observational Results & Data Analysis

On 20 February 2002, RHESSI observed a C7.5 flare in NOAA active region 9825, located near the northwest limb of the Sun at N16W80 (919″W, 285″N). The GOES-8 soft X-ray flare started at 11:02 UT and ended at 11:12 UT. The RHESSI hard X-ray peak time was at 11:06:20 UT, as shown in Figure 1.

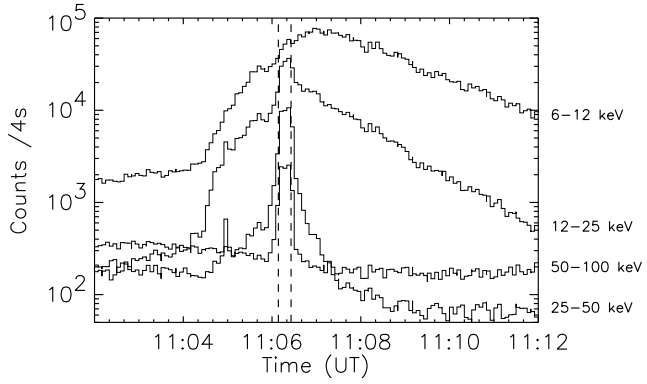

Figure 1. RHESSI light curves in four energy bands. The count rate (4 s time integration) is summed over detectors 1 through 9, excluding detectors 2 and 7. For clarity, we have scaled the count rates by 5.0 (6–12 keV), 1.5 (12–25 keV), 1.0 (25–50 keV), and 1.0 (50–100 keV). The two vertical lines show the integration time interval for the RHESSI images and spectra in this paper.

The spatially integrated and background-subtracted photon spectrum at the time of the hard X-ray peak, 11:06:10 – 11:06:24 UT

(see Fig. 1), is shown in Figure 2. This spectrum was obtained using the RHESSI spectral executive (SPEX) software (see Smith *et al.*, 2002). We have integrated a program into SPEX that computes the thick-target bremsstrahlung flux spectrum from a single or a double power-law distribution of electrons. The photon spectrum in Fig. 2 was obtained by fitting the RHESSI count data to the bremsstrahlung spectrum from an isothermal plasma plus a double power-law electron distribution.

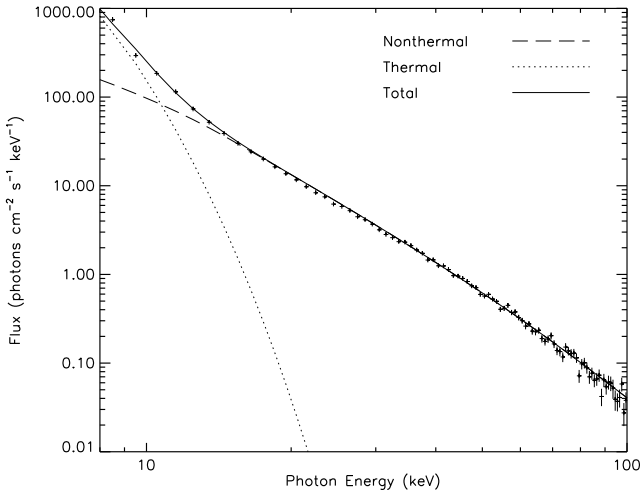

Figure 2. RHESSI spatially integrated, background-subtracted photon spectrum for the time interval 11:06:10 – 11:06:24 UT, the same as that for all RHESSI images shown later. The bremsstrahlung spectrum from an isothermal plasma plus a double power-law electron distribution (both shown separately on the plot, in addition to the total spectrum) were fit to the RHESSI count data to obtain this spectrum.

The background varied with time during this flare. It was subtracted from the flare data by obtaining a linear fit to measurements of the background flux before and after the flare. Below 100 keV uncertainties in the fluxes resulting from the background subtraction are less than 20%.

The RHESSI thin shutters were in the field of view of the detectors for this event. When the thin shutters are in, the e ective area of the detectors drops rapidly as the photon energy falls below 10 keV. The current uncertainty in the correction factor is large at these energies, so fluxes below 10 keV were not included for spectral fitting. The X-ray background flux becomes significant at photon energies above 100 keV, so fluxes at energies above 100 keV were also not included.

The emission measure and temperature determined from our fit to the spatially integrated RHESSI spectrum in Fig. 2 are 2×10^{48} cm^{-3} and 15 MK, respectively. We obtained an emission measure and

temperature from the GOES-8 soft X-rays data at 11:06:20 UT of 3×10^{48} cm^{-3} and 14 MK. These were determined using the program GOES_TEM.PRO in the Solar Software Tree, which was developed from the concepts of Garcia (1994) and Thomas, Crannell, and Starr (1985). The GOES-8 results are consistent with those from our spectral fit to the RHESSI data.

We have found several functions that provide a good fit to the non-thermal part of the spatially integrated spectrum. The double power-law fit to the photon spectrum included with SPEX gives a spectral index of -3.3 below 56 keV and -4.3 above 56 keV. The normalization of the double power-law fit is 0.6 photons s^{-1} cm^{-2} keV^{-1} at 50 keV. We have verified the existence of this break in the photon spectrum by analyzing the data from each individual detector.

The fit shown in Fig. 2 is the bremsstrahlung spectrum from a double power-law electron density distribution. This gives a power-law index for the electron distribution of -4.4 below 100 keV and -5.5 at higher energies. With a low-energy cuto in the distribution at 15 keV, the normalization gives the total suprathermal electron density times source area to be $nA = 4.6 \times 10^{25}$ electrons cm^{-1}. The low-energy cuto was chosen to be 15 keV because this minimizes the total number of suprathermal electrons while still providing a good fit to the photon spectrum. The bremsstrahlung from a single power-law density distribution with a high-energy cuto also provides a good fit to the data. This gives a power-law index of -4.5 and a high-energy cuto of 224 keV. The value of nA is the same as before.

A single power-law electron distribution with a low-energy cuto at 47 keV also provides an acceptable fit to the spectrum. The power-law index is -5.3 and $nA = 1.24 \times 10^{24}$ electrons cm^{-1}. But this fit requires a much higher temperature for the thermal plasma, 40 MK, with an emission measure of 4.6×10^{46} cm^{-3}. Since this temperature and emission measure do not correspond to the results from GOES, this case will not be pursued further here, but will be explored in future work.

RHESSI images (see Hurford *et al.*, 2002) in six energy bands at the time of the hard X-ray spike are plotted in Figures 3 and 4. Each image is 64×64 arcseconds in size. At the time of this analysis, the relative alignment was not known for collimators 1 and 2, so the spatial resolution of the images is limited to 7″. Collimator 9 was also not included, since all source structure was well below 180″ in extent.

In order to check the reliability of di erent image reconstruction algorithms, images using both the Maximum Entropy (MEM-Sato – Figure 3) and the CLEAN (Figure 4) reconstruction techniques were obtained. MEM-Sato is an image reconstruction algorithm utilizing the

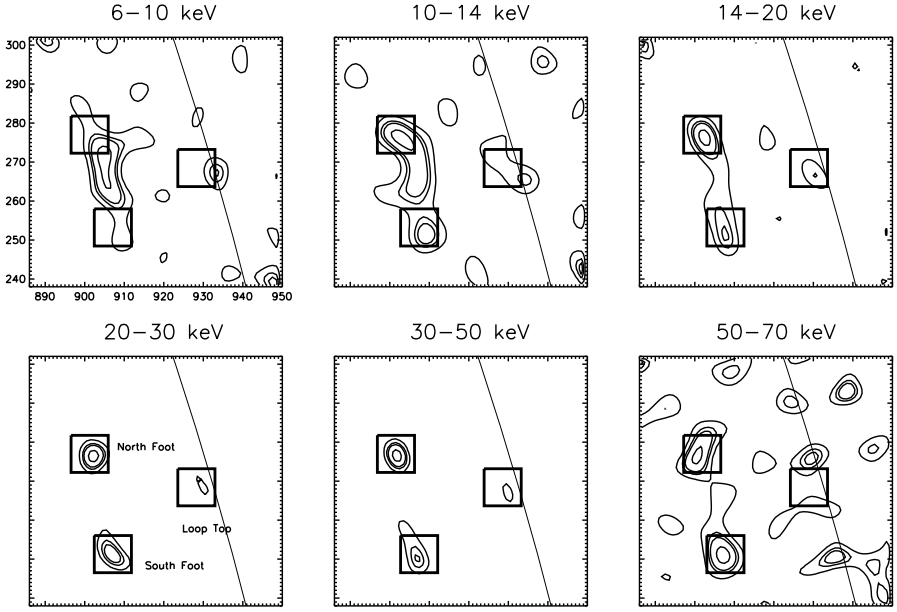

Figure 3. Images obtained with the MEM-Sato algorithm. The time interval is 11:06:10 UT – 11:06:24 UT. The contour levels are 0.08, 0.2, 0.3, 0.7. The contour levels are normalized to the peak flux of each image. The smooth line shows the location of the solar limb. The three boxes indicate the pixels that were summed to obtain the footpoint and looptop spectra in Fig. 5.

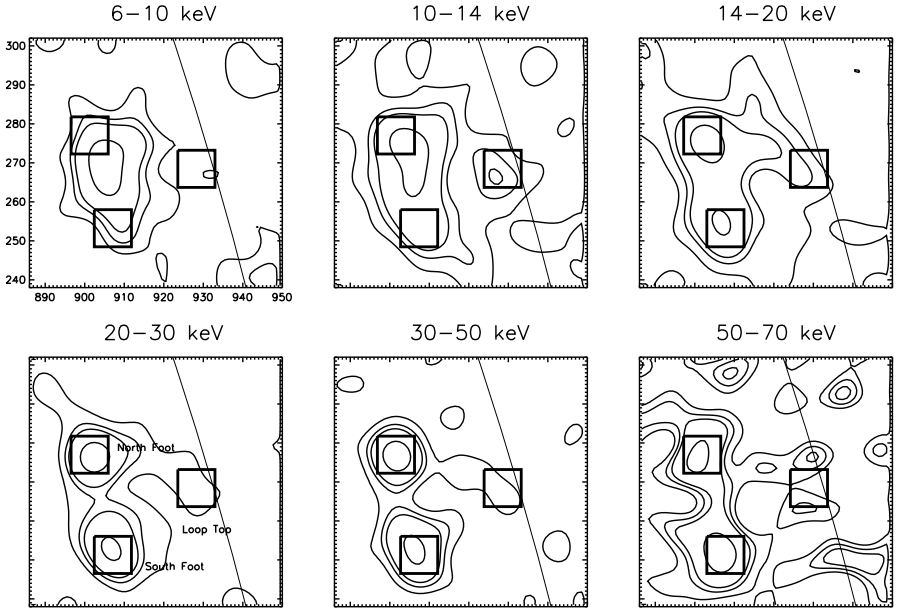

Figure 4. Images obtained with the CLEAN algorithm. All other aspects are the same as in Fig. 3.

maximum entropy method (MEM) described by Sato *et al.* (1999), modified for RHESSI. The clean algorithm is an iterative procedure that takes the dirty map, made using back projection (Hurford *et al.*, 2002), finds the brightest pixel, and uses some fraction of its intensity and point spread function to subtract side lobes from the dirty map. This process is then repeated until the brightest pixel is negative, or a maximum number of iterations has been reached. The CLEAN and MEM-Sato images agree with each other in coarse structure. In the low energy band (6–10 keV), the images show a single source which lies between the two footpoints observed at higher energies. This is identified to be a thermal source with a temperature of 15 MK. In the 10–14 keV band, the images show the thermal source and a possible looptop source. In the energy bands between 14 keV and 50 keV, the images show two separate footpoints and the looptop source. In the 50–70 keV band the looptop source is not present in the images. The quality of the images in this energy band is marginal, however, because of the low count rate.

In order to obtain the spectral characteristics of the footpoints and looptop, we integrated the flux within an $8'' \times 8''$ box around each of the two footpoints and the looptop (see Figs. 3 & 4). This box size was chosen to encompass the total emission from each feature.

We found the results from MEM-Sato and CLEAN to be similar. Spectra of the footpoints (left panel) and the looptop (right panel) obtained from the CLEAN maps are shown in Figure 5. Since the two footpoints have similar spectra, we just plot the north footpoint and the looptop source. The results from the data are shown as horizontal bars marked with an "x". The width of the bar indicates the width of the energy band. The bars marked with diamonds are from the flare model (see Section 4 below).

The immediately apparent result from these spectra is that the looptop spectrum is softer than the footpoint spectra. A rough power-law fit to these spectra gives a spectral index of -3 for the footpoints and -4 for the looptop. This di erence of one in spectral index is consistent with a recent statistical analysis of limb flares observed by *Yohkoh* (Petrosian, Donaghy, and McTiernan, 2002). At 6–10 keV, the flux from the north footpoint is higher than the extrapolated power-law. This is because the thermal source between the footpoints is closer to the north footpoint, and the thermal source contributes to the flux from the north footpoint in this energy band. Since the looptop source does not appear in the images at 50–70 keV, the spectral fitting does not include this energy band.

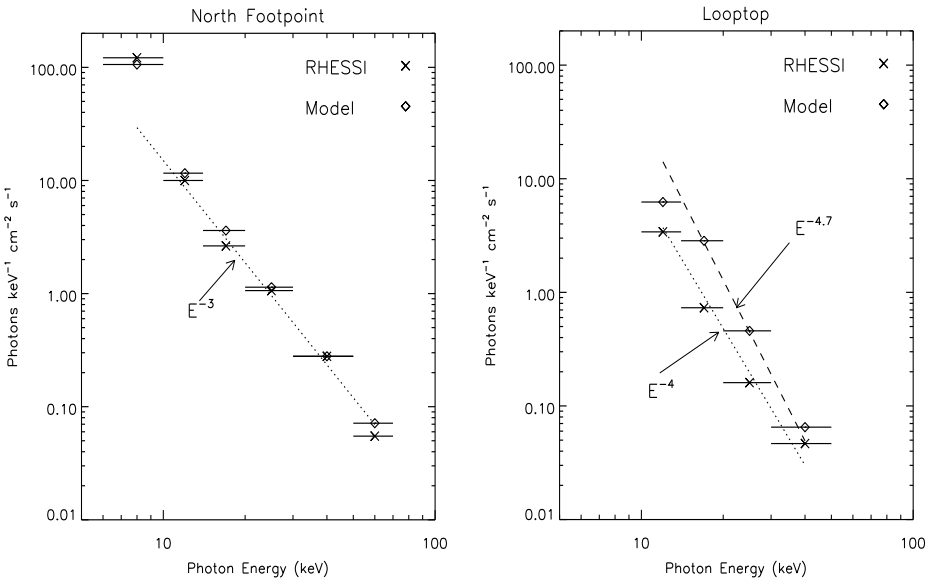

Figure 5. Spectra for the north footpoint (left panel) and looptop (right panel). The horizontal bars marked with an "x" are from the CLEAN images shown in Fig. 4. The bars marked with a diamond are from the model images reconstructed with CLEAN (Fig. 9). The time interval is the same as that for Figures 3 and 4.

3. Flare Model

In the model, we assume that electrons with a power-law energy distribution and an isotropic pitch-angle distribution are injected at the top of a single semicircular flare loop. The steady-state electron spatial and spectral distributions within the loop were obtained with a Fokker-Planck code (McTiernan and Petrosian, 1990). The code includes Coulomb scattering and energy losses and magnetic mirroring. We computed the hard X-ray emission from the coronal loop and footpoints using thin-target and thick-target bremsstrahlung radiation codes. Hot plasma is assumed to uniformly fill the flare loop. Based on the flare images shown in Figures 3 and 4, we added a thermal source between the two footpoints.

The radius of the semicircular loop in the model is 17″, and the diameter of the magnetic tube is 4″. The magnetic field is assumed to be uniform (constant) along the length of the flare loop so that magnetic mirroring of the energetic electrons does not occur. The plane of the loop must be rotated 53° from the plane of the sky to match the flare geometry in the RHESSI images.

The density distribution of the nonthermal electrons injected at the looptop is determined by the fit to the spatially integrated photon

spectrum: the nonthermal electron power-law spectral index is -4.4 between 15 keV and 100 keV and -5.5 above 100 keV, and the total electron density is 3.5×10^8 cm^{-3}. The plasma density and temperature within the loop are 3.5×10^{10} cm^{-3} and 10 MK, respectively. The loop would be too bright, i.e., would be seen with RHESSI, if its temperature were much greater than 10 MK at this density.

The thermal source between the footpoints is taken to be 20″ long, 4″ wide, and 4″ deep. The thermal source is shifted 5″ toward the north footpoint from the center of the two footpoints. This configuration was chosen to provide images that agree reasonably well with the RHESSI images. The plasma density and temperature of this thermal source were chosen to agree with the results of the spectral fit: 1.4×10^{11} cm^{-3} and 15 MK.

Images at 6, 15 and 50 keV from the model are shown in Figure 6. These images are shown with one arcsecond spatial resolution. At 6 keV, the thermal source between the two footpoints is very strong compared with the footpoints and the looptop source. The flare loop is nearly invisible at this energy because emission from the loop is weaker than that from the central thermal source. At 15 keV, the thermal source between the footpoints disappears. The looptop and footpoint sources are visible. Only the two footpoint sources are visible at 50 keV.

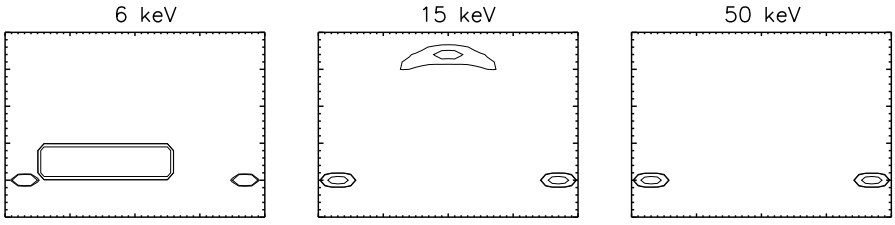

Figure 6. Model flare loop images at 6 keV, 15 keV and 50 keV. Contour levels are 0.05, 0.07, and 0.5 times the peak flux in each image. The spatial resolution is 1″. These images are not rotated and scaled to the RHESSI images.

Looptop and footpoint spectra from the model are plotted in Figure 7. The footpoint fluxes are obtained by summing over all pixels that show emission from one footpoint. The looptop fluxes are obtained by summing over 32 pixels at the top of the model loop. The thermal emission at low energies (dotted curve) is from the model loop, not the thermal source between the footpoints. The spectral index of the footpoints is -3.1 between 15 keV and 56 keV, and -4.4 above 56 keV. The spectral index of the looptop is -5.0 between 15 keV and 56 keV, and -5.7 above 56 keV. Comparing the model spectra with the data, the spectral index of the footpoints from the model below 56 keV agrees

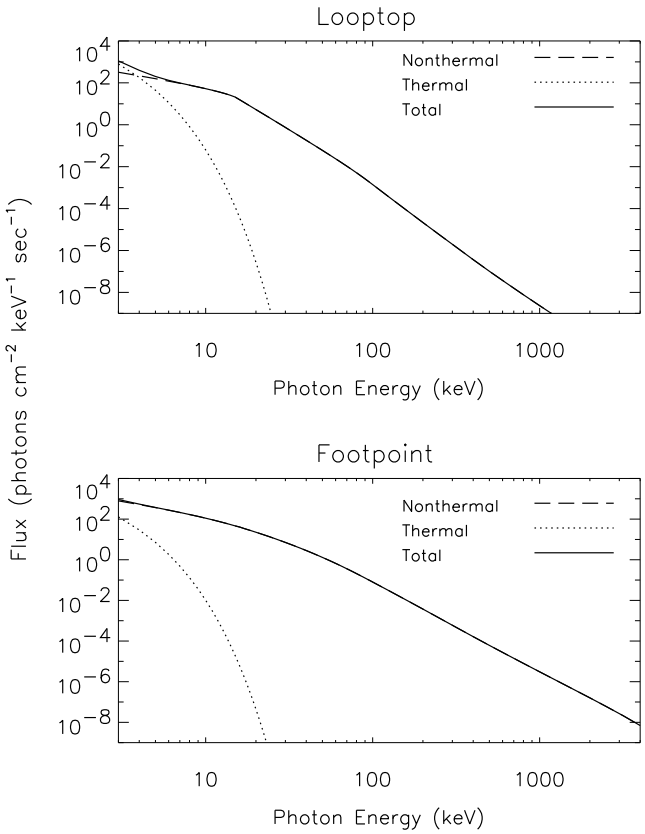

Figure 7. Spectra from the model loop images. The top panel shows the spectrum from the looptop and the bottom panel shows the spectrum from a footpoint. The dashed curve is the total nonthermal bremsstrahlung from a footpoint or the looptop, the dotted curve is the thermal bremsstrahlung from the same region, and the solid curve is the total spectrum.

with our estimated index, -3, from the RHESSI imaging spectra. The spectral index of the looptop is higher than the value of -4 estimated from the data, however.

4. Simulation Results and Analysis

The RHESSI imaging software allows us to input our flare model to obtain simulated images. This allows us to compare simulated images with RHESSI images to test our model. It also allows us to check the imaging software itself to identify possible artifacts from the image reconstruction process. We input each model image as a 64×64 array

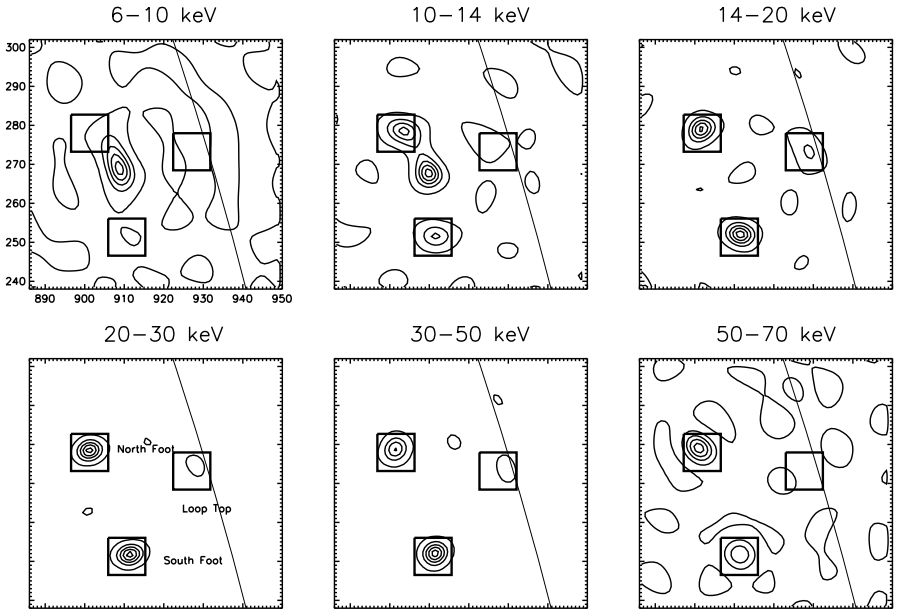

Figure 8. MEM-Sato images of the model flare loop. Contour levels are 0.1, 0.3, 0.5, 0.7, and 0.9. The contours are normalized to the peak flux of each image. As in Figures 3 & 4, the smooth line is the solar limb.

into the imaging software. All imaging parameters are the same as those used for the RHESSI images. As shown in Figures 8 and 9, the simulated MEM-Sato and CLEAN images roughly agree with the images of Figures 3 and 4. At 6–10 keV, only the thermal source between the two footpoints is visible. At 10–14 keV, the thermal source still dominates. Note that in the MEM-Sato images, the uniform thermal source appears to be a double source. There is a weak looptop source visible in both the MEM-Sato and CLEAN images. At 14–20, 20–30 and 30–50 keV, two clear-cut footpoints and a looptop source are visible. This agrees with the RHESSI images. At 50–70 keV, the looptop source vanishes and only the two footpoints are still visible.

With this simple simulation process, we have found that both the MEM-Sato and the CLEAN imaging algorithms can alter the relative brightness of the flare components. An example of this is shown in Figure 10. An unprocessed image from the model is shown in the top left panel. This 14–20 keV model image was not used in simulating the RHESSI data because the looptop is too bright. This same image processed with MEM-Sato and with CLEAN are shown in the bottom left and bottom right panels. It was processed in the same way as the other images, including only grids 3 through 8. The upper right panel

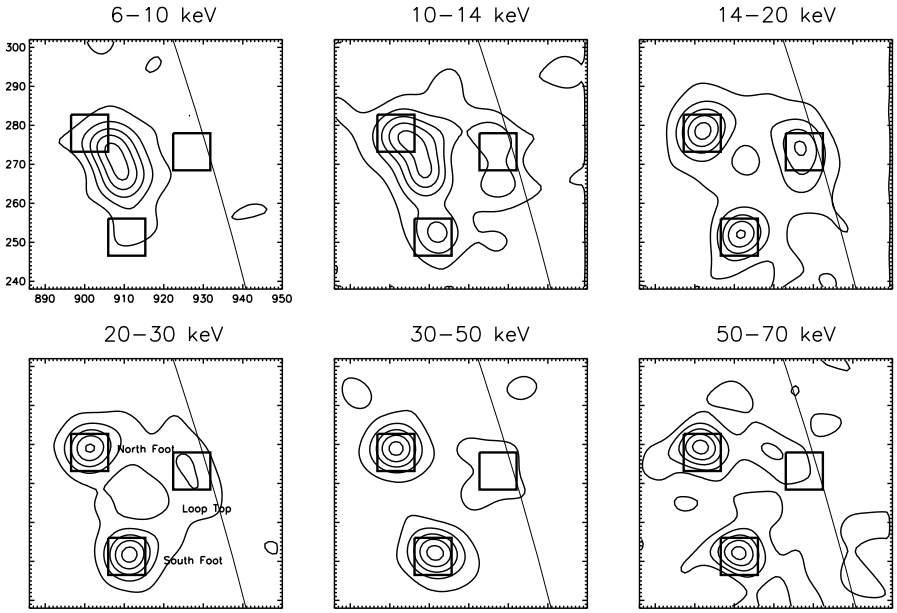

Figure 9. CLEAN images of the model flare loop. Contour levels are the same as Fig. 8.

shows the model image smoothed with a conical response function with a full width at half maximum of 7″. This simulates the lower resolution of the processed images. In the unprocessed image, the peak flux from each footpoint is about 2 times higher than that from the looptop. In the other three images, however, the peak flux of the looptop is about 2 times higher than that of the footpoints. This is because the looptop source is more extended than the footpoints, and the spatial averaging at the lower spatial resolution picks up flux from many pixels in the looptop while the footpoint emission originates from only a few pixels.

As is the case for the unprocessed model image, the north and the south footpoints have about the same peak flux in the smoothed and the CLEAN images. In the MEM-Sato image, however, the peak flux of the north footpoint is 30% higher than that of the south footpoint. For all the images, however, the integrated flux from the north footpoint is about the same as the integrated flux from the south footpoint. MEM-Sato has super-resolved the X-ray sources — they are more compact than the spatial resolution of the instrument. On the other hand, compared to the smoothed image, CLEAN has enhanced the emission from the southern leg of the loop relative to the peak flux from the footpoints by about 130%. Fortunately most of these discrepancies are relatively small, but they could be di cult to recognize in RHESSI images without comparing the images with model images.

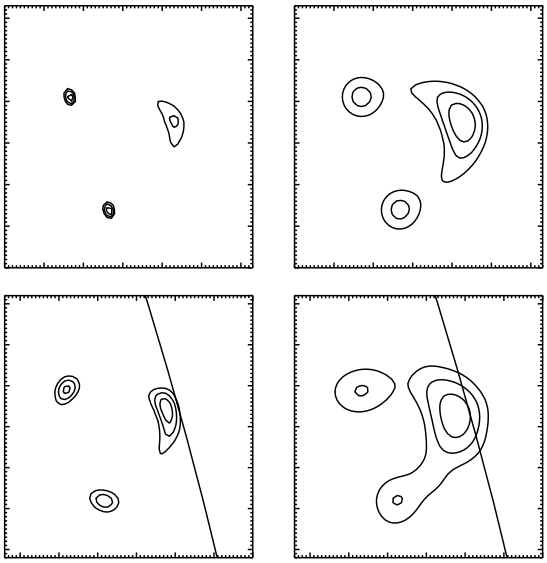

Figure 10. An unprocessed image from the flare model (top left), the same image convolved with a 7″ FWHM conical response function (top right), the same image processed with MEM-Sato (bottom left), and the image processed with CLEAN (bottom right) are shown. Contour levels are 0.2, 0.4, and 0.7 times the peak flux in each image.

Figure 11 shows a simulated image from the model processed with MEM-Sato on the left (Fig. 8, 14–20 keV) and the corresponding MEM-Sato flare image on the right (Fig. 3, 14–20 keV). For clarity, an additional low-flux contour (0.05) has been added to the RHESSI map from Fig. 3. Some artificial sources appear in the simulated image. Comparing the simulated MEM-Sato image with the RHESSI MEM-Sato image, we can see similar patterns in both images. Consequently, we deduce that these "sources" between the footpoints and the coronal source in the RHESSI flare image are also not real.

Spectra obtained from these simulated images from the model are shown in Figure 5 along with the spectra obtained from the RHESSI flare images. The fluxes from the model are marked with diamonds. Lacking error bars for the fluxes deduced from the flare images, we do not yet have a meaningful, quantitative test of goodness of fit. Nevertheless, the footpoint spectrum can be seen to be closely reproduced by the model. The looptop spectrum, on the other hand, is poorly reproduced. The model spectrum is too steep relative to the flare data. The looptop spectrum for the flare can be fitted with a power-law spectral index of about -4, while the spectral index of the model (15 keV to 50 keV) is about -4.7. We have not found a way to rectify this problem without significantly changing the physical model.

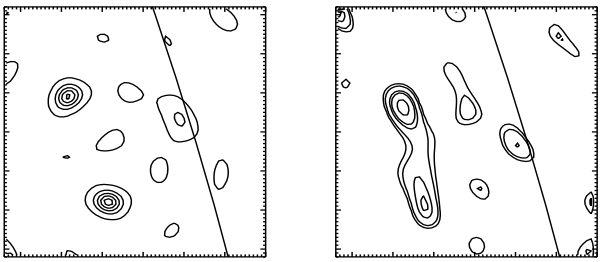

Figure 11. MEM-Sato 14–20 keV images of the model (left) and of the observed flare (right). We can see similar patterns in them. The sources between the looptop and footpoints in the left image are not real. Consequently, we deduce that sources between the footpoints and the looptop in the right image are also not real.

Fig. 5 shows that the looptop flux from the model is too high at low energies. The flux at, say, 14–20 keV could be brought into agreement with the flux from the flare by deceasing the plasma density in the loop. At higher energies the looptop source would be too weak, however, and would not be visible in the simulated images.

5. Discussion and Conclusions

Our results indicate that the simple flare model applied here does not adequately describe the X-ray emission from the 20 February 2002 flare. In this model the looptop and footpoint X-ray sources arise from the injection of suprathermal electrons at the top of a magnetic loop. The lower energy electrons in the injected particle distribution interact with the loop plasma to produce the looptop source, while the footpoint sources are produced when the particles reach the high-density footpoints of the loop (Holman, 1996). The problem with the model is that the looptop flux decreases more rapidly with increasing photon energy than indicated by the spectrum obtained from the RHESSI images.

Another issue that at first appears to be inconsistent with the model is the relative timing of the brightening of the north and south footpoints. Figure 12 shows the time history of the emission from each footpoint in the 20–25 keV energy range. The time of peak emission for the north footpoint is about 8 s earlier than that of the south footpoint. Since the time required for a 25 keV electron with a pitch angle of 45° to travel from the top of the loop to a footpoint is only 0.4 s, our simple model does not provide an explanation for this substantial time delay. Higher spatial resolution maps indicate, however, that the southern footpoint is actually two distinct footpoints that reach peak brightness at di erent times (Krucker and Lin, 2002). The peak emission from the

northern footpoint appears to be cotemporal with the peak of the emission from the northern component of the southern footpoint. The peak in the emission from the southern component of the southern footpoint is cotemporal with a secondary peak in the emission from the northern footpoint. Therefore, the timing does not appear to be inconsistent with the electron propagation time. The relative timing and brightness of the footpoint pairs still require an explanation, however.

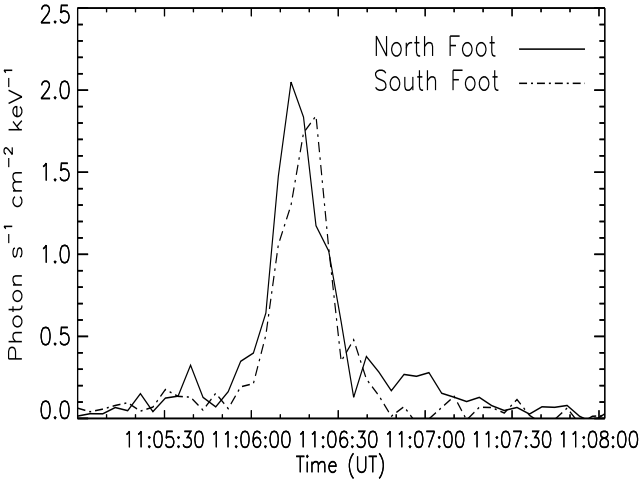

Figure 12. Emission history of the two footpoints at 20–25 keV. The start time is 11:05:00 UT. The peak of the north footpoint emission is earlier than the peak of the south footpoint emission by about 8 seconds.

We have found that the comparison of RHESSI images with images generated from a model provides a valuable check on the image reconstruction process. We found that this comparison allowed us to identify spurious sources and enhanced source fluxes in the reconstructed maps. We also found that the MEM-Sato algorithm misrepresented the uniform thermal source included in the model, displaying it as a double source rather than an elongated single source.

Given the low flux of the looptop source relative to the footpoints, its reality must be questioned. Our use of two di erent image reconstruction techniques and comparison with the simulated maps from the model indicate that it is a real source, however. Also, post-flare loops observed with the SOHO EIT indicate the presence of a loop extending from the hard x-ray footpoints to the looptop source (see Fig. 4 of Krucker and Lin, 2002).

The thermal source between the footpoints was an unexpected feature of the flare emission. This source dominated the thermal radiation from the flare. This would not have been unexpected if we had been looking down on a flare loop on the disk of the Sun. It is an unexpected

feature, however, for a loop at the limb of the Sun with a looptop source displaced toward the limb. We found the thermal source to be located closer to the northern hard x-ray footpoint than the southern footpoint. It is interesting that the northern footpoint was also the first to reach peak brightness. It is likely that this thermal source was a low-lying loop interacting with the northern footpoint of the higher loop containing the looptop source. The northern component of the southern footpoint is likely to have been the southern footpoint of this low-lying loop.

A significant handicap we faced for this analysis was the lack of knowledge of the uncertainties in the fluxes obtained from the RHESSI images (Fig. 5). Without a knowledge of these uncertainties, we could not properly evaluate the ability of the model to fit the imaged spectra. Our future work will include a careful evaluation of the imaging and the simulation processes to establish a realistic estimate of these uncertainties. This will include obtaining images using the PIXON method (Metcalf et al., 1996). The PIXON method requires more time to produce an image, but an estimate of the uncertainties is provided by the algorithm and the photometry is expected to be better.

We will also seek out refinements to our model and to other models that may provide a more acceptable description of the observational results from this and other flares observed by RHESSI. Other particle injection and propagation models that include a density enhancement (Wheatland and Melrose, 1995) or magnetic trapping (Fletcher and Martens, 1998) at the top of the loop are likely to su er the same problem with the looptop spectrum as the model applied here. If this problem is not resolved, the most likely conclusion is that suprathermal electrons are accelerated in the looptop source and/or elsewhere in the observed flare loop.

The temperature of 10 MK or less deduced for the loop containing the looptop source is rather low for a flare loop. Heating of the loop plasma by the suprathermal electrons alone, especially in the region of the looptop source, can be quite high. We will explore models that include a hotter plasma, perhaps confined to the looptop region, to determine if they can be consistent with the RHESSI results.

We found several functions that provided a good fit to the spatially integrated flare spectrum. For weak to moderate intensity flares such as the flare analyzed here, the flux typically becomes undetectable above the background at energies below 200 keV. These flares are amenable to a wider variety of spectral fits than more intense flares for which the spectrum can be established up to energies of 500 keV or above. Our future studies will include the analysis of these more intense flares that have now been observed by RHESSI.

This work was supported in part by the NASA Sun-Earth Connection Program and the RHESSI Project. This work would not have been possible without the dedication, hard work, and support of the entire RHESSI team. We especially thank Paul Bilodeau for his help in integrating the thick-target bremsstrahlung code with the SPEX software, and Ed Schmahl for several helpful discussions. We thank the referee, James McTiernan, and the "uno cial RHESSI referee," Hugh Hudson, for their helpful comments on the paper.

References

Fletcher, L., and Martens, P. C. H.: 1998, *Astrophys. J.* 505, 418.
Garcia, H.: 1994, *Solar Phys.* 154, 275.
Holman, G. D.: 1996, *B.A.A.S.* 28, 939; also see http://hesperia.gsfc.nasa.gov/sftheory/loop.htm.
Holman, G.D., Mariska, J.T., McTiernan, J.M., Ofman, L., Petrosian, V., and Ramaty, R.: 2001, *BAAS* 33, 1444; also see http://hesperia.gsfc.nasa.gov/hessi/modelware.htm.
Holman, G.D., Sui, L., McTiernan, J.M., and Petrosian, V.: 2002 Theoretical Model Images and Spectra for Comparison with HESSI and Microwave Observations of Solar Flares, *Yohkoh 10th Anniversary Meeting Proceedings* , in press.
Hurford, G., *et al.*: 2002, *Solar Phys.*, this volume.
Krucker, S., and Lin, R. P.: 2002, *Solar Phys.*, this volume.
Masuda, S.: 1994, *Nature* 371, 495.
Masuda, S.: 2002, Hard X-ray Solar Flares Revealed with Yohkoh HXT – A Review, *Yohkoh 10th Anniversary Meeting Proceedings*, in press
McTiernan, J. M., and Petrosian, V.: 1990, *Astrophys. J.* 359, 524.
Metcalf, T. R., Hudson, H. S., Kosugi, T., Puetter, R. C., and Pina, R. K.: 1996, *Astrophys. J.* 466, 585.
Petrosian, V., Donaghy, T. Q., and McTiernan, J. M.: 2002, *Astrophys. J.* 569, 459.
Sato, J., Kosugi, T., and Makishima, K.: 1999, *Publ. of the Astronomical Society of Japan* 51, 127.
Smith, D., *et al.*: 2002, *Solar Phys.*, this volume.
Thomas, R. J., Crannell, C. J., and Starr, R.: 1985, *Solar Phys.* 95, 323.
Wheatland, M. S., and Melrose, D. B.: 1995, *Solar Phys.* 158, 283.